Rheol. Acta **10**, 344–364 (1971)

From the Pulp and Paper Research Institute of Canada, and Department of Chemistry, McGill University, Montreal (Canada)

Particle motions in non-Newtonian media

I: Couette flow*)

By F. Gauthier, H. L. Goldsmith, and S. G. Mason

With 14 figures and 6 tables

(Received September 25, 1970)

List of symbols

a; $a'(\varphi_1)$ = semi axis of revolution of spheroids; projection of this axis on the X_2X_3-plane at φ_1.
A = function of r_e defined by equation (20).
b; $b'(\varphi_1)$ = radius of a rigid sphere, undeformed drop and semi axis of equatorial diameter of rigid cylinder; projection of this axis on the X_2X_3-plane at φ_1.
B = minor axis of a deformed liquid drop.
C, C_0; C' = orbit constant, orbit constant at $t = 0$; dynamic orbit constant.
D = geometrical deformation of a fluid drop.
E; E_B = calculated deformation of a fluid drop; deformation at burst.
F = total normal force measured in the rheogoniometer.
$f(\lambda)$ = $(19\lambda + 16)/(16\lambda + 16)$.
G, $G(R)$; G_B = velocity gradient, at R in the *Couette* annulus; value of G at burst.
G' = measured velocity gradient.
h = height of liquid in the *Couette* apparatus.
K, n = constants for power law fluid.
L = major axis of a deformed drop.
p_{23}, $p_{33} - p_{22}$ = tangential shear stress; normal stress difference.
r_p = particle axis ratio = a/b.
r_e = equivalent ellipsoidal axis ratio.
r_{23}, $\bar{r}_{23}$ = projection and average projection of unit length of rod axis on the X_2X_3-plane.
R; R_{I}, R_{II} = radial distance of the particle center from the axis of rotation in *Couette* flow; radius of inner and outer cylinder of *Couette* apparatus.
R_c = radius of the cone of the rheogoniometer.
R_{23} = axis ratio of the ellipse, projection of particle rotational orbit in the X_2X_3-plane.
t = time.
T = period of rotation of particle.
U_3 = fluid velocity along X_3-axis.
X_1, X_2, X_3 = *Cartesian* coordinate axes of the external flow field.
ΔX_2, ΔX_3 = distances along the X_2 and X_3 axes of a sphere center from the mid-point of the collision doublet axis.
α = rheological constant.
α_2 = spheroid integral.
$\varkappa$ = $\gamma/Gb\,\eta_0$.
λ = viscosity ratio = η_1/η_0.
η_0, η_1 = respective apparent viscosities of the suspending and suspended phases.
γ = interfacial tension.
τ = total torque applied on the liquid in a *Couette* apparatus.
θ_1, φ_1 = spherical polar coordinates referred to the polar axis X_1 of the external flow field.
φ_a, φ_r = rectilinear angles of approach and recession of collision doublet of rigid spheres.
φ_m = φ_1-orientation of principal axis of deformed drop in shear flow.
ω_1 = angular velocity of a spheroid.
$\Omega(R)$; Ω_{I}, Ω_{II} = angular velocity of the fluid at R; angular velocities of the inner and outer cylinders of the *Couette* apparatus.
Γ_1 = hydrodynamic torque.

Introduction

A series of investigations conducted in this laboratory have described the behaviour of rigid and deformable particles suspended in *Newtonian* liquids undergoing *Couette* and *Poiseuille* flow at very low *Reynolds* numbers. Beginning with single isolated particles studies were made of the rotations of rigid spheres, discs and rods, the different modes of deformation and break-up of liquid drops, and the orbits of rotations of flexible filaments. Particle interactions in dilute suspensions were then studied by observing two- and three-body collisions between spheres, and by measuring the transient and steady state orientations of cylinders. A comprehensive review of this work and the underlying theory has recently been given (1).

The motions of single rigid and deformable particles have since been observed in sheared elasticoviscous

*) This work was supported by the Defence Research Board of Canada (DRB Grant 9530-47).

liquids[1]) made by dissolving polyisobutylene in decalin or polyacrylamide in water (2). The present investigation represents an extension of this phase of the work to the slow *Couette* flow of pseudoplastic liquids, i. e. liquids which exhibit a continuous decrease in viscosity with increasing rate of shear without any appreciable elastic recovery when the shearing action is stopped. Included in the experiments are measurements of the rotation, migration, deformation and two-body collisions of spheres and cylinders as well as a study of the deformation of elasticoviscous drops and aspects of particle interactions in elasticoviscous fluids, hitherto not examined. Similar experiments in tube flow will be described in a forthcoming publication (4).

It should be pointed out that whereas in *Newton*ian media, the particle motions can be predicted from the linearized *Navier-Stokes* equation with solutions given by *Jeffery* (5), *Brenner* (6) and *Taylor* (7), no such theory exists to describe the sometimes different behaviour in elasticoviscous and pseudoplastic suspending fluids. It has been suggested that some of these flow properties are a result of the combined action of normal stresses and the velocity gradient (2, 8). Hence, evidence for the existence of normal stresses in the suspending phase solutions was sought from measurements carried out in a rheogoniometer. In addition the shear rate – shear stress relationships were determined in each case. Pseudoplastic liquids follow the so-called "power law" (9), which in terms of the right-handed *Cartes*ian coordinate system X_1, X_2, X_3 of the external flow field, defined by $U_3 = GX_2$ as shown[2]) in fig. 1a, may be written:

$$p_{23} = KG^n. \qquad [1]$$

Here p_{23} is the tangential shear stress (fig. 1b), G is the rate of shear, and K and n are two constants depending on the fluid. When $n = 1$, this equation reduces to *Newton*'s law with $K = \eta$, the viscosity; when $n > 1$, the liquid is termed dilatant and when $n < 1$, pseudoplastic. As a consequence of eq. [1], the velocity profile in a liquid flowing under conditions of variable shear is different from that in a *Newton*ian fluid. Although not as pronounced as in *Poiseuille* flow, this effect would be expected in the case of *Couette* flow in the annulus between two counter-rotating cylinders considered in the present work.

[1]) Following the terminology suggested by *Reiner* and *Scott Blair* (3), the liquids designated "viscoelastic" in reference 2 are here termed "elasticoviscous".

[2]) In this convention, based on the usual right-handed coordinate system, X_1 is parallel to the vorticity axis; the velocity filed is parallel to the X_3-axis instead of along the X_1-axis as is often used in rheology.

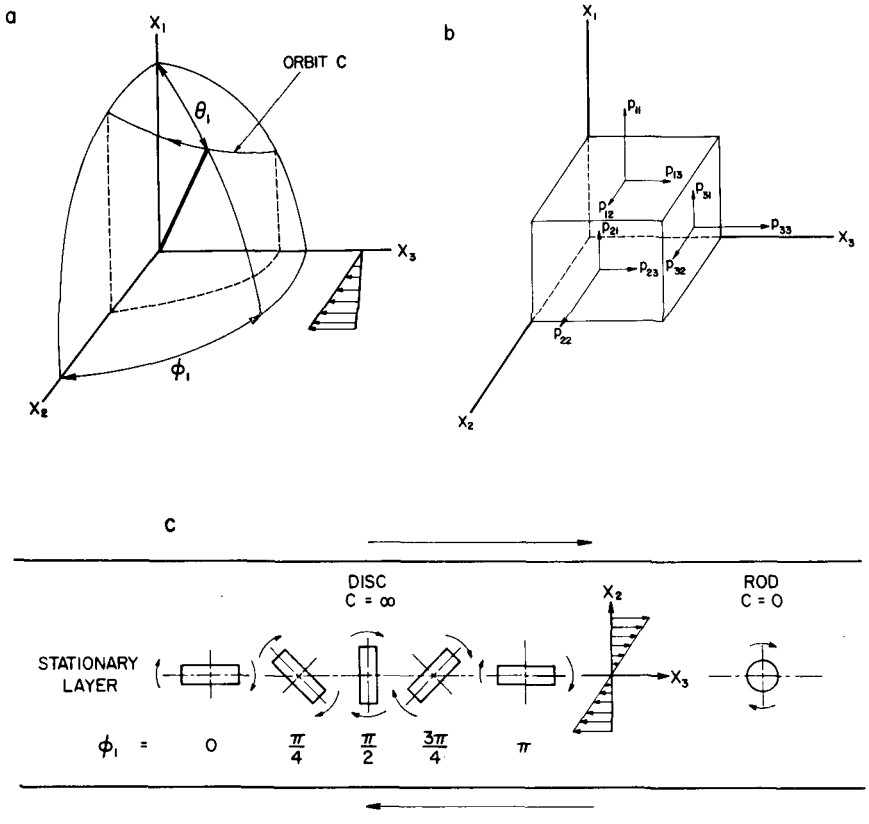

Fig. 1. (a) *Cartes*ian coordinate system X_1, X_2, X_3 of the external flow field. θ_1 and φ_1 are the polar coordinates with respect to X_1 as the polar axis. The upper end of the axis of revolution of a prolate spheroid ($r_e > 1$) is shown tracing out the path of a spherical elliptical orbit having the orbit constant C. – (b) Stresses acting on three faces of a unit cube in a *Cartes*ian coordinate system X_1, X_2, X_3; p_{11}, p_{22} and p_{33} are the normal stress components and p_{ij}, $(i \neq j)$, are the tangential (or shear) stress components. – (c) Projections of a disc (left) and a rod (right) rotating in *Couette* flow viewed along the X_1-axis after they have attained orbits having the respective limiting values $C = \infty$ and 0

The results described below show, however, that some of the observed phenomena, such as the migration of rigid spheres toward a region of higher shear in the *Couette* apparatus, and the unsymmetrical two-body collisions cannot at present be adequately interpreted in terms of the known rheological properties of the fluids used.

Experimental part

The experiments were made in a *Couette* apparatus previously described (10) in which the suspensions were sheared in the annulus between two counter-rotating cylinders. The particle motions were viewed through a microscope aligned with the axis parallel to the planes of shear and recorded with a Paillard Bolex camera mounted on the microscope. The cine films were subsequently analysed on a drafting table.

The pseudoplastic liquids were obtained by dissolving a carboxyvinyl polymer (Carbopol 940, B. F. Goodrich Chemical Company) in water, glycerine, ethylene glycol, propylene glycol or a mixture of these, giving solutions from 0.07 to 0.15% by weight of polymer. The resin was supplied as a powder in acid form and was mixed by stirring into the solvent until completely dissolved. The solution was then neutralized with few drops of sodium hydroxide or triethylamine to the accompaniment of a marked increase in viscosity.

Aqueous elasticoviscous solutions were prepared by dissolving a high molecular weight polyacrylamide supplied as a white powder (Cyanamer P250, Polyacrylamide, American Cyanamid Company) at concentrations ranging from 1 to 4%. These solutions when stirred mechanically showed the *Weissenberg* climbing effect (11), while the pseudoplastic liquids did not have this property. The elastic behaviour of the polyacrylamide solutions was also evident when small tracer polystyrene spheres were suspended in the liquids being sheared in the *Couette* apparatus with one cylinder stationary. When the other cylinder was suddenly stopped, the particles showed translational recovery in a direction opposite to that of the flow. This behaviour was not observed with particles suspended in the pseudoplastic solutions.

The $p_{23} - G$ relations for these liquids, shown in fig. 2a were measured in a rotational viscometer (Epprecht Rheomat 15). The apparent viscosities of all the liquids decreased with increasing G and the solutions of carboxyvinyl polymers were found to follow eq. [1] in agreement with the observations of *Metzner* and *Dodge* (12). Carbopol solutions had previously been studied by *Fisher, Bauer* and *Wiberley* (13), who reported that they could "... clearly establish the presence of a yield stress for concentrations only above 0.5%", the value being 60 dyne cm^{-2} at $p_H = 6.6$ and 25 °C. However, nothing is recorded in the literature for the lower concentrations used in this study (< 0.2%). None of the solutions studied in the present work were thixotropic or rheopectic i.e. the measured shear stresses did not change with time and at a given G were identical after increasing or decreasing the shear rates.

The normal stresses were measured at room temperature (25 °C) with a *Weissenberg* rheogoniometer (Sangamo Controls Ltd.) equipped with a flat plate and a 1° cone of 5.0 cm of diameter[3]). The results for

[3]) These experiments were carried out with the instrument of Dr. *A. L. Copley* at the Veterans Hospital, East Orange, N. J. The authors are most grateful to Dr. *Copley* for permission to use the rheogoniometer and to Mr. *King* who kindly supervised the measurements.

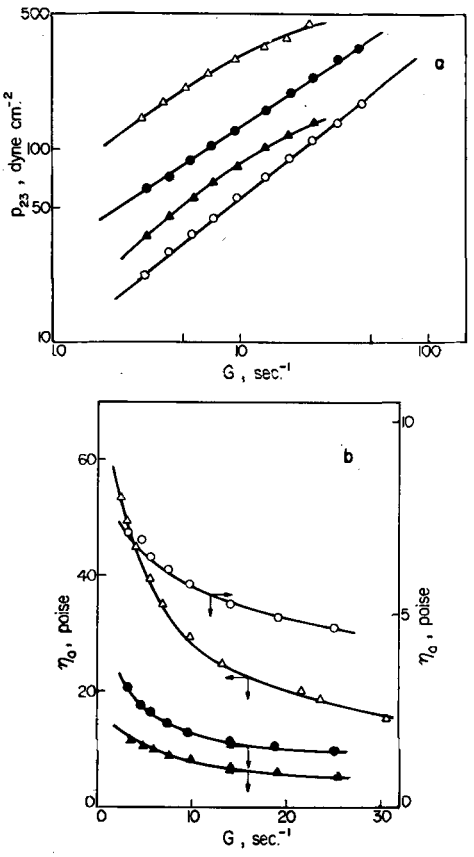

Fig. 2. (a) Log-log plot of the shear stress (dyne cm^{-2}) against the rate of shear (sec^{-1}) for two pseudoplastic liquids: open circles, system 1; closed circles, system 8; and two elasticoviscous liquids: open triangles, system 8; and two elasticoviscous liquids: open triangles, system 10; and closed triangles, system 18. There were no suspended particles in these liquids. – (b) Apparent viscosities as a function of the shear rate for the same systems

the polymer solutions at three concentrations over a range of G from 2 to 200 sec^{-1} are illustrated in fig. 3, where the pressure difference $p_{33} - p_{22}$ was calculated from the total force F applied on the cone of radius R_c using the equation:

$$p_{33} - p_{22} = \frac{2F}{\pi R_c^2}. \qquad [2]$$

With polyacrylamide solutions, appreciable normal stresses existed at shear rates < 5 sec^{-1} and increased with increasing G and concentration of polymer in solution. For example, in a 1% solution at $G = 5.5$ sec^{-1}, $p_{33} - p_{22}$ was 0.3 dyne cm^{-2}, but in 2 and 3% solutions at a lower G of 2.2 sec^{-1} it reached 2.2 and 4.5 dyne cm^{-2} respectively.

In the case of the pseudoplastic solutions, no normal stresses were apparent at velocity gradients below 50 sec^{-1}. At higher rates of shear, normal stresses were detected when the rheogoniometer was switched on, but they decreased slowly as secondary flows developed. In all cases the normal stresses were very small, decreasing from 2.5 dyne cm^{-2} at $G = 217$ sec^{-1} to only 0.2 dyne cm^{-2} at $G = 68$ sec^{-1}, a value which was of

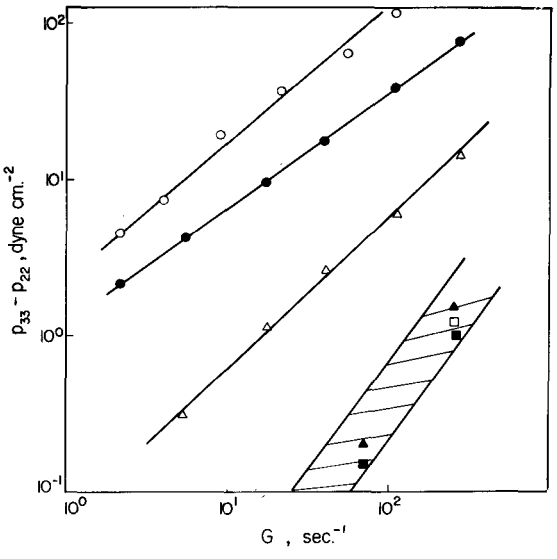

Fig. 3. Normal stresses as a function of the shear rate for three elasticoviscous solutions of polyacrylamide in water: open circles, 3% by weight; closed circles, 2% by weight; open triangles, 1% by weight, and three pseudoplastic solutions: closed triangles, 0.2% by weight, $n = 0.79$; open squares, 0.15% by weight, $n = 0.88$; closed squares, 0.1% by weight, $n = 0.90$. Because of the experimental error in the measurements for the pseudoplastic solutions, the points are enclosed in the hatched area

the same order of magnitude as the sensitivity of the apparatus. Due to the uncertainty in the measurements the data for the pseudoplastic liquids in fig. 3 are shown enclosed between two parallel lines. Since all the experiments described below were carried out at $G < 8$ sec^{-1}, the existence of measurable normal stresses in the pseudoplastic liquids is ruled out.

Lists of the different systems and their properties are given in tables 1 and 2 for suspensions of rigid and deformable particles respectively. The velocity profiles were determined with small aluminum tracer particles; polystyrene spheres, discs, and nylon rods

Table 1. Suspensions of rigid particles.
Pseudoplastic media: carboxyvinyl polymer in alcohols; concentration = 0.07 to 0.15% by weight

System	Solvent	K dyne sec^n cm^{-2}	n	η_0*) Poise	Suspended phase	Range of particle dimensions $\times 10^3$ cm
1					aluminum particles	< 2
2	propylene glycol	10.2	0.77	7.26	nylon rods	a = 25 to 53 b = 2 to 3
3					polystyrene discs	a = 6 to 8 b = 46 to 72
4	propylene glycol	9.8	0.79	6.91	polystyrene spheres	b = 32 to 56
5	propylene glycol	6.8	0.87	5.42	polystyrene spheres	b = 67
6	ethylene glycol	32.4	0.62	22.2	polystyrene discs	a = 7 b = 57
7					polystyrene spheres	b = 58
8	propylene glycol and glycerine	30.6	0.63	20.4	polystyrene spheres	b = 40 to 55

Elasticoviscous medium: polyacrylamide in water

System	Solvent	concentration (by weight)	η_0*) Poise	Suspended phase	Range of particle dimensions $\times 10^3$ cm
9	water	0.025	20.2	polystyrene sphere	b = 67
10	water	0.030	49.7	aluminum particles	< 2
11	water	0.030	49.7	nylon rod	a = 52 b = 4
12	water	0.040	150.5	polystyrene disc	a = 6.5 b = 54

*) Apparent viscosity measured at $G = 3.11$ sec^{-1} except for systems 10 and 12 where $G = 2.18$ sec^{-1}.

Table 2. Suspensions of deformable particles

System	Suspending phase	η_0 [1] Poise	Suspended phase	η_1 [1] Poise	λ	γ dyne cm^{-1}	b mm	Deformation class
13	Pseudoplastic:	16.3	dibutylphthalate	0.21	0.01	< 2	0.50–0.73	B–1
14	carboxyvinyl	16.3	Ucon oil LB 1715 [2]	1.49	0.08	2	0.58–0.69	B–1
15	polymer in	16.3	silicone oil (200 fluid) [3]	0.10	0.006	7.5	0.80	B–1
16	propylene glycol	16.3	silicone oil (200 fluid) [3]	5.08	0.37	7.5	0.65	B–1
17 [4]	$n = 0.71$ $\varkappa = 22.9$ dyne sec^n cm^{-2}	16.3	silicone oil (510 fluid) [3]	0.51	0.03		0.66–0.91	—
18 [4]	Elasticoviscous: polyacrylamide in water ($c = 0.015$)	11.5	silicone oil (510 fluid) [3]	0.51	0.04		0.43–0.83	—
19	Newtonian:	53.1	propylene glycol	0.24	0.004	8.6	0.63	A
20	Silicone oil (510 fluid)[3]	53.1	carbopol in propylene glycol ($n = 0.71$), $\varkappa =$ 22.9 dyne sec^n cm^{-2}	16.3	0.31	8.6	0.63–0.86	B–1
21		53.1	carbopol in propylene glycol ($n = 0.97$), $\varkappa =$ 1.1 dyne sec^n cm^{-2}	1.32	0.02	8.6	0.92	B–1
22		53.1	carbopol in propylene glycol ($n = 1.0$), $\varkappa = 0.8$ dyne sec^n cm^{-2}	0.84	0.015	8.6	0.88	B–1
23		53.1	water	0.01	2×10^{-4}	21.2	0.81	A
24		53.1	1.5% by weight polyacrylamide in water	11.5	0.22	19.4	0.74	B–1
25		53.1	4% by weight polyacrylamide in water	150.5	2.84	16.5	0.54–0.88	B–2

[1]) For the non-*Newtonian* liquids, η_0 and η_1 represent the apparent viscosities measured at $G = 3.110$ sec^{-1}, except for system 25 where $G = 2.927$ sec^{-1}.
[2]) Union Carbide, polyglycol oils.
[3]) Dow Corning Silicone Fluids (Series 200 and 510 fluid).
[4]) Systems 17 and 18 were used for the study of the migration of drops.

being used to study particle rotation, migration and collision.

Systems 13 to 18 in table 2 were made up by dispersing *Newtonian* drops in non-*Newtonian* liquids, and vice versa in systems 19 to 25. The liquid drops were released from a hypodermic syringe immersed in the suspending phase, and pictures were taken before and during deformation. The interfacial tensions were measured with a DuNouy tensiometer except for systems 24 and 25 where the elastic properties of the liquid might have influenced the readings. Here the measurements were made using the rotating drop method (14), in which a fluid drop of known volume is suspended in an horizontal tube filled with a denser and immiscible liquid. As the tube rotates, the drop assumes an axisymmetric position and is elongated along the axis of rotation until the deformation forces due to the centrifugal field are balanced by the interfacial tension. From the measured drop length and volume, speed of rotation and density differences between the two phases, the interfacial tension can be calculated.

Except for the normal stress measurements, all the experiments were made in a thermostated room at 22 ± 0.5 °C.

Results and discussion

a) Velocity profiles

The velocity profiles in a pseudoplastic (system 1) and elasticoviscous liquid (system 10) were determined by measuring the translational velocities of small aluminum particles and are in fig. 4.

For a fluid located in the annulus two concentric cylinders of radius R_I and R_{II}, rotating with respective angular velocities Ω_I and Ω_{II}, the velocity gradient G at radial distance R in cylindrical coordinates is given by:

$$G = -R\frac{d\Omega(R)}{dR}, \qquad [3]$$

where $\Omega(R)$ is the angular velocity of the fluids.

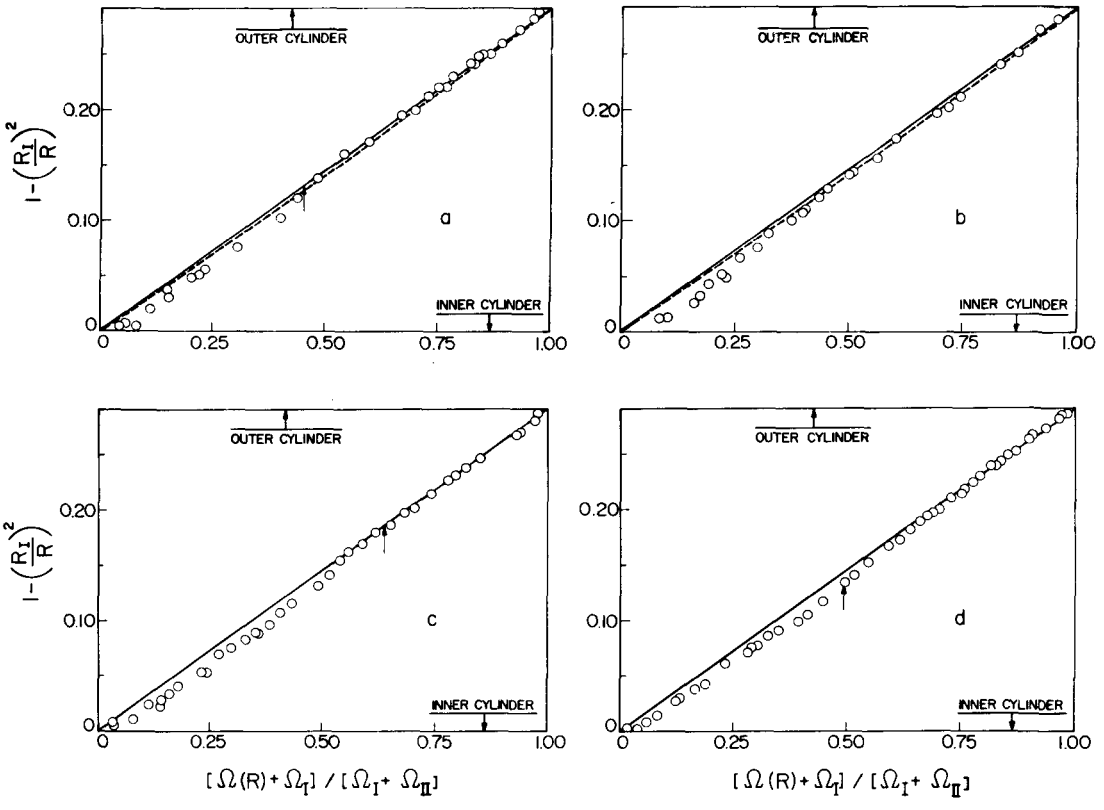

Fig. 4. Velocity profiles of non-*Newton*ian liquids in *Couette* flow. $R_I = 4.756$ cm, $R_{II} = 5.652$ cm. – Pseudoplastic liquid, system 1: (a) $\Omega_I = 0.011$ rad. sec^{-1}, $\Omega_{II} = -0.013$ rad. sec^{-1}; (b) $\Omega_I = 0.045$ rad. sec^{-1}, $\Omega_{II} = 0$. Elasticoviscous liquid, system 10: (c) $\Omega_I = 0.014$ rad. sec^{-1}, $\Omega_{II} = -0.007$ rad. sec^{-1}; (d) $\Omega_I = 0.030$ rad. sec^{-1}, $\Omega_{II} = -0.031$ rad. sec^{-1}. – The positive and negative signs refer to counterclockwise and clockwise rotation respectively. The solid line represents the velocity profile of a *Newton*ian liquid and the dashed lines in (a) and (b) were calculated from equation [6] with $n = 0.77$. The points are experimental. The arrows give the location of the stationary layer in the annulus

If τ is the total torque applied on the liquid, and h its height in the annulus, then the shear stress at R is:

$$p_{23} = \frac{\tau}{2\pi R^2 h}. \qquad [4]$$

For a power law liquid, we may apply eq. [1] and substitute it, with eq. [4], into eq. [3] to obtain:

$$\frac{d\Omega(R)}{dR} = -\left(\frac{\tau}{2\pi K h}\right)^{1/n} \cdot \frac{1}{R^{\frac{2+n}{2}}}. \qquad [5]$$

Integration of eq. [5] with the boundary conditions

$$\text{when } R = R_I,\ \Omega(R) = \Omega_I,$$
$$\text{and when } R = R_{II},\ \Omega(R) = \Omega_{II},$$

then yields:

$$\frac{\Omega(R) + \Omega_I}{\Omega_I - \Omega_{II}} = \frac{R_{II}^{2/n}}{R_{II}^{2/n} - R_I^{2/n}} \left(1 - \frac{R_I^{2/n}}{R^{2/n}}\right). \qquad [6]$$

For two counter-rotating cylinders, the velocity gradient at the stationary layer is:

$$G(R) = \frac{2}{n} \frac{\Omega_I R_I^{2/n} - \Omega_{II} R_{II}^{2/n}}{R_{II}^{2/n} - R_I^{2/n}}. \qquad [7]$$

When the liquid is *Newton*ian, $n = 1$ in eqs. [6] and [7] (15).

In figs. 4a and 4b, the solid lines represent the velocity profile for a *Newton*ian liquid while the dashed lines were calculated from eq. [7] for the pseudoplastic media using the measured $n = 0.766$. Despite the fact that n was appreciably different from unity, it is evident that the two velocity profiles are very close together and the scatter in the experimental points is such that they give a good fit with either line. A small but significant deviation from the *Newton*ian velocity profile was however obtained for the elasticoviscous liquid (fig. 4c and 4d). At the stationary layer indicated by the arrows in the figure, the

velocity gradients calculated from eq. [7] assuming *Newtonian* behaviour were slightly greater than those, G', calculated from the slope of the best fit line drawn through the experimental points. For fig. 4c, $G'/G = 0.94$, and for fig. 4d, $G'/G = 0.98$.

b) Rotation of particles

The angular velocities of rigid spheres, discs and rods and the orientations of the cylinders were studied over a range of G from 0.1 to 2 sec^{-1}. In the spherical polar coordinates shown in fig. 1a with X_1 as the polar (and also the viewing) axis, the rotation of the axis of revolution of spheroids suspended in a *Newtonian* liquid is described by *Jeffery*'s equations (5):

$$\omega_1 = \frac{d\varphi_1}{dt} = \frac{G}{r_p^2 + 1}(r_p^2 \cos^2\varphi_1 + \sin^2\varphi_1), \quad [8]$$

$$\frac{d\theta_1}{dt} = \frac{G(r_p^2 - 1)}{4r_p^2 + 1}\sin 2\varphi_1 \sin 2\theta_1, \quad [9]$$

where G is the velocity gradient, θ_1 and φ_2 are the polar angles defined in fig. 1a and r_p is the axis ratio (axis of revolution/equatorial diameter) $= 2a/2b$.

(i) *Spheres:* For a sphere, $r_p = 1$ and eq. [8] reduces to:

$$\omega_1 = \frac{G}{2}, \quad [10]$$

a relation which has been verified experimentally for *Newtonian* liquids (15). The steady angular velocities of spheres suspended in a pseudoplastic medium [system 5 ($n = 0.87$)] given in table 3, were also in good agreement with the values calculated from the experimental G and eq. [7], the mean $2\omega_1/G$ being 0.99 ± 0.03.

Table 3 also compares the observed angular velocities of spheres in an elasticoviscous fluid with those calculated assuming *Newtonian* behaviour of the fluid. It is evident that the values were slightly less than the theoretical with a mean $2\omega_1/G = 0.95 \pm 0.02$. It was not possible to compute $2\omega_1/G'$ since the velocity profiles were not measured, but the decrease is of the same order as that of G'/G measured at the stationary layer in system 9. Thus, it is probable that $2\omega_1/G' = 1$ and the results show that the rotation of the field is equal to half the velocity gradient.

(ii) *Rods and discs, angular velocity:* The variation of the angle φ_1 with time of rigid cylinders in the pseudoplastic systems 2 and 3, illustrated in fig. 5a, was obtained from the cine films by measuring the angle

Table 3. Comparison between the calculated and observed angular velocities of spheres in non-*Newtonian* liquids

Pseudoplastic liquid system 5, $n = 0.87$			Elasticoviscous liquid system 9		
$2\omega_1$ obs. rad. sec^{-1}	G calc.[1] sec^{-1}	$\frac{2\omega_1(\text{obs.})}{G}$ (calc.)	$2\omega_1$ obs. rad. sec^{-1}	G calc.[2] sec^{-1}	$\frac{2\omega_1(\text{obs.})}{G}$ (calc.)
0.122	0.13	0.98	0.179	0.19	0.96
0.175	0.19	0.95	0.297	0.29	1.03
0.265	0.27	0.98	0.368	0.39	0.96
0.312	0.33	0.96	0.447	0.50	0.90
0.427	0.43	1.00	0.644	0.70	0.92
0.542	0.52	1.04	0.818	0.85	0.97
0.555	0.53	1.05	0.963	1.02	0.95
0.580	0.58	1.00	1.08	1.16	0.93
0.624	0.65	0.98	1.28	1.36	0.94
0.705	0.73	0.92	1.55	1.78	0.98
0.728	0.74	0.99	2.04	2.18	0.94
0.789	0.75	1.04		Average:	0.94
0.904	0.88	1.02		Mean deviation:	± 0.02
0.907	0.92	0.98			
0.955	0.93	1.02			
1.17	1.07	1.09			
1.07	1.11	0.96			
1.15	1.19	0.97			
0.977	1.00	0.98			
1.55	1.48	1.04			
	Average:	0.99			
	Mean deviation:	± 0.03			

[1]) Using eq. [7] with $n = 0.87$.
[2]) Using eq. [7] assuming *Newtonian* behaviour, $n = 1$.

of the major axis of the particle with the wall of the *Couette* cylinder as the reference X_3-axis (fig. 1a). As previously found in elasticoviscous solutions, and predicted by eq. [8], $d\varphi/dt$ in each orbit is a minimum for a rod at $\varphi_1 = \pi/2,\ 3\pi/2$ and for a disc at $\varphi_1 = 0, \pi$. Again as in elasticoviscous liquids, there was a continuous drift of the variation of the angle θ_1 with time, and the particles finally took on limiting rotational orbits which are described below.

Integration of eq. [8] yields:

$$\tan\varphi_1 = r_p \tan\frac{2\pi t}{T}. \quad [11]$$

where T is the period of rotation about the X_1-axis. Eqs. [8] and [11], applicable to ellipsoids of revolution, have also been verified for rigid rods (15) and discs (16), providing an equivalent ellipsoidal axis ratio r_e, instead of r_p is used, r_e being calculated from the measured T by means of the relation:

$$T = \frac{2\pi}{G}\left(r_e + \frac{1}{r_e}\right). \quad [12]$$

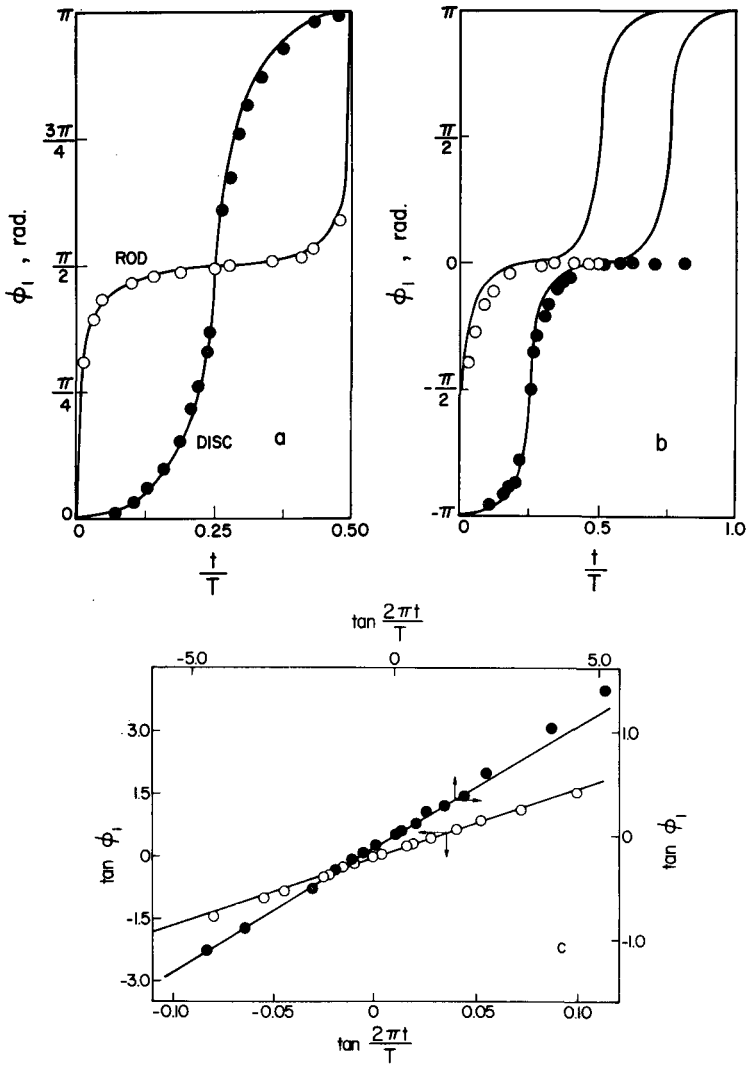

Fig. 5. (a) Variation of φ_1 with time for a rigid rod and a rigid disc in a pseudoplastic solution. Rod: open circles, $r_p = 23.2$, $r_e = 16.1$, $G = 0.57\,\text{sec}^{-1}$, system 2. Disc: closed circles, $r_p = 0.11$, $r_e = 0.24$, $G = 1.17\,\text{sec}^{-1}$, system 3. (b) Variation of φ_1 with time for a disc in an elasticoviscous solution, system 12, $r_p = 0.12$, $r_e = 0.15$. Open circles: $G = 1.04\,\text{sec}^{-1}$; closed circles: $G = 0.31\,\text{sec}^{-1}$. The curves are calculated from eq. [11] using the experimental r_e obtained for the same disc in a *Newton*ian liquid. When $\varphi_1 = 0$, the discs, now aligned with the flow, did not rotate further. – (c) Variation of tan φ_1 with tan $2\pi t/T$ according to eq. [11] for the same rod and disc shown in (a) with the same conditions. The lines drawn were calculated using r_e obtained from the experimental T and G in a *Newton*ian liquid

It can be seen from figs. 5a and 5b that the results, using the experimental r_e, are in excellent agreement with eqs. [8] and [11]. As previously found in *Newton*ian and elasticoviscous media, the equivalent ellipsoidal axis ratios of the particles determined from eq. [12] using the experimental values, of T and G were greater than the particle axis ratios r_p for the discs and smaller than r_p for the rods. The values when inserted into a plot of r_e/r_p versus $\log r_p$ given in fig. 6 lie close to the best fit line drawn from data of previous investigations in *Newton*ian liquids (16, 17), the scatter at low r_p presumably being due to some small imperfections in the shape of the discs.

(iii) *Rods and discs: Drift in the orbit constant* When eq. [9] is integrated, one obtains

$$\tan\theta_1 = \frac{Cr_e}{(r_e^2\cos^2\varphi_1 + \sin^2\varphi_1)^{1/2}}, \qquad [13]$$

where C is the orbit constant which can assume values between 0 and ∞. It follows from eq. [13] that

$$\text{at}\quad \varphi_1 = \frac{\pi}{2}, \quad \tan\theta_1 = Cr_e,$$

$$\text{and at}\quad \varphi_1 = 0, \quad \tan\theta_1 = C. \qquad [14]$$

Experimentally, the angle θ_1 was computed from the following relations:

$$\frac{a'(\varphi_1)}{a} = \sin\theta_1,$$

$$\frac{b'(\varphi_1)}{b} = \cos\theta_1, \qquad [15]$$

$2a'(\varphi_1)$ and $2b'(\varphi_1)$ being the respective projected lengths of the axis of revolution and equatorial diameter on the X_2X_3-plane.

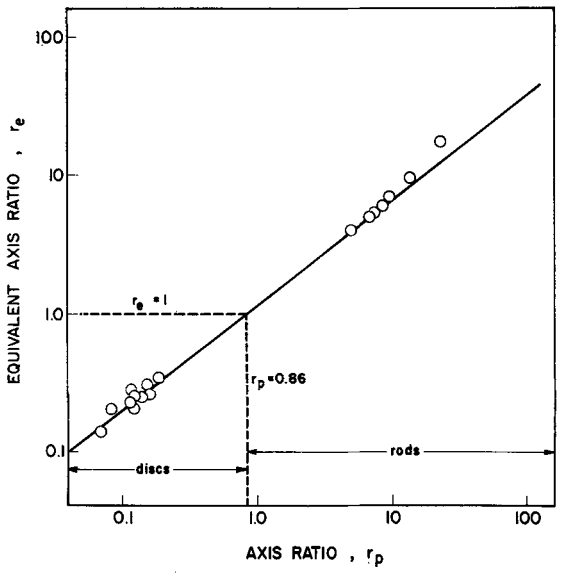

Fig. 6. Equivalent ellipsoidal axis ratio r_e, as a function of the particle axis ratio r_p for rods and discs in pseudoplastic liquids. The points are experimental (system 2, 3 and 6) and the line is drawn from reference (17) and is the best fit of several studies carried out in *Newton*ian liquids

The above theory, applicable in the *Stokes* or creeping flow regime, does not predict the existence of preferred orbits (5). This was confirmed by experiments at very low *Reynolds* numbers in *Newton*ian liquids in which the orbit adopted by a rod or disc was found to depend only on the initial conditions of release (16, 18); the particle then continued to rotate without change of orbit, provided it did not sediment or collide with other cylinders. However, in elasticoviscous fluids (2), drifts in the orbit constant were observed such that the particles took on limiting rotational orbits as illustrated in fig. 1c with $C = 0$ for a rod and $C = \infty$ for a disc. Similar drifts were here observed in the pseudoplastic systems 2 and 3. To distinguish the transient or dynamic orbit constant, obtained from solutions of eq. [13] at a given t/T, from the true orbit constant, C is replaced by C' below. In the final orientations as illustrated in fig. 1c, a rod spins about its long axis which is aligned parallel to the X_1-axis, and a disc rotates in the edge-on position with its axis of revolution in the X_2X_3-plane. A convenient way of presenting the drift in orbit is to plot the projection of the axis of revolution in the X_2X_3-plane. For a constant orbit C, the projection is an ellipse of axis ratio R_{23} given by (19):

$$R_{23} = \left(1 + \frac{1}{C^2}\right)^{1/2} \left(1 + \frac{1}{C^2 r_e^2}\right)^{-1/2}. \qquad [16]$$

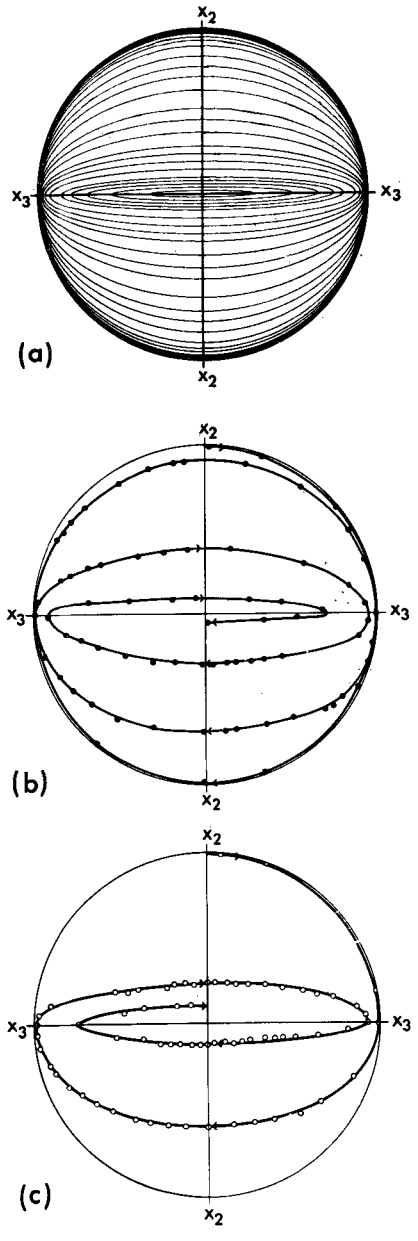

Fig. 7. (a) Calculated and computer-drawn X_2X_3-projections of the axis of revolution of a rod (= semi-major axis) with $r_e = 16.1$ in various spherical elliptical orbits whose constant C increases from 0 at the origin, to the circle corresponding to $C = \infty$. – (b) and (c) Respective measured projections of one end of the same rod suspended in an elasticoviscous liquid ($G = 0.53\,\mathrm{sec}^{-1}$, system 11) and in a pseudoplastic liquid ($G = 0.57\,\mathrm{sec}^{-1}$, system 2) showing the progressive drift of the orbit constant from $C' = \infty$ to C' close to 0 in the direction given by the arrows. The lines are the best fit of the experimental points

When $r_e > 1$, the major axis lies along the X_3-axis and when $r_e < 1$, it lies along the X_2-axis. At $C = \infty$, $R_{23} = 1$ and the projection is a circle, the center of which re-

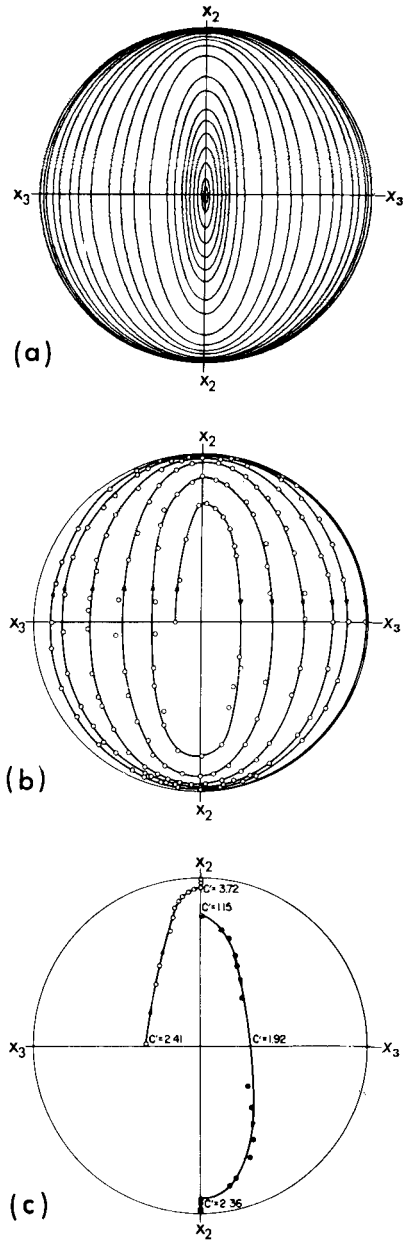

Fig. 8. (a) Calculated and computer-drawn X_2X_3-projections of the axis of revolution (= semi-minor axis) of a disc with $r_e = 0.24$ rotating in various spherical elliptical orbits. At the origin $C = 0$; the circle corresponds to $C = \infty$. (b) Measured projections of one end of the axis of revolution of the same disc suspended in a pseudoplastic liquid ($G = 1.11$ sec^{-1}, system 3) as the orbit constant drifted from a value initially close to $C' = 0$ to $C' = \infty$ in the direction given by the arrows. – (c) Measured projections for disc, $r_e = 0.15$ suspended in an elasticoviscous liquid. Same particle and conditions as in fig. 5b. In (b) and (c), the lines are the best fit through the experimental points

presents the projection at $C = 0$. Figs. 7a and 8a show a set of ellipses calculated and drawn with the aid of an IBM 360 computer for various C in the case of a rod with $r_e = 16.1$ and a disc $r_e = 0.24$ assuming no change in C with time. The actual time course of the dynamic orbit constant C' for the same rod as in fig. 7a is shown in figs. 7b and 7c in elasticoviscous and pseudoplastic liquids respectively. Starting with an orientation where C' was large, the curves appear as concentric spirals with the biggest change in C' occurring when φ_1 is within $\pm 10°$ of $\pi/2$ or $3\pi/2$ where the particle spent 80% of its time, very little decrease in C' occurring in the rest of the orbit. A similar plot was obtained for a disc suspended in a pseudoplastic solution. Here, as illustrated in fig. 8b, C' increased from an initial value close to 0 to a final value at infinity, and as expected, the major change in C' occurred while the particle was close to the orientations $\varphi_1 = 0$ and π. In all cases, the drifts were rapid, taking only between 2 and 3 rotations for the rod at $G = 0.57$ sec^{-1}, and 5 to 6 rotations for the disc at $G = 1.1$ sec^{-1}, to reach the limiting orientations in the propylene glycol solution.

In a theoretical study, *Saffman* (20) showed that in non-*Newton*ian liquids, a particle could assume preferred orbits but was unable to predict in which direction C' would vary. He derived the following relation for the rate of change in C':

$$\frac{1}{C'}\frac{dC'}{dt} = \frac{G^2\,\alpha}{\eta_0}\,f(C'/a), \qquad [17]$$

where α is a constant characterizing the non-*Newton*ian properties of the liquid and $f(C'/a)$ is a function depending on the particle shape and on the rate of strain tensor. A plot of $\ln C'/C_0$ against time according to the integrated form a eq. [17], with C_0 the orbit constant at time $t = 0$, is given in fig. 9 for different cylinders suspended in elasticoviscous and pseudoplastic liquids. The experimental points at each r_e and G fall on straight lines suggesting that the function $f(C'/a)$ in eq. [17] is a constant for a given system in the range of variation of C' observed: $C'/C_0 < 10$ for discs and $C'/C_0 > 0.03$ for rods. As C' approached the limiting value, $a'(\varphi_1)/a$ in the case of rods and $b'(\varphi_1)/b$ in the case of discs became very close to 0. Hence θ_1 from eq. [15] and C' could no longer be computed with any accuracy and eq. [17] could no longer be verified. In both elasticoviscous and pseudoplastic liquids, dC'/dt increased with the velocity gradient. In all these

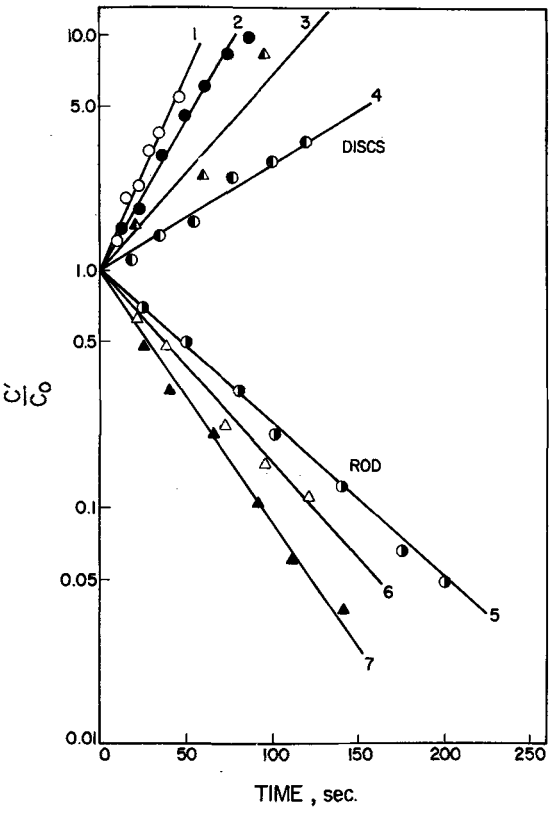

Fig. 9. Variation of $\log C'/C_0$ with time for a rod $r_e = 16.1$ and different discs rotating in pseudoplastic and elasticoviscous liquids. The lines drawn are the best fit of the experimental points.
1: disc, $r_e = 0.22$, $G = 2.38\,\text{sec}^{-1}$, $C_0 = 0.75$, system 6.
2: disc, $r_e = 0.24$, $G = 1.11\,\text{sec}^{-1}$, $C_0 = 0.66$, system 3.
3: disc, $r_e = 0.15$, $G = 0.31\,\text{sec}^{-1}$, $C_0 = 1.15$, system 12.
4: disc, $r_e = 0.22$, $G = 0.71\,\text{sec}^{-1}$, $C_0 = 0.89$, system 6.
5: rod, $G = 0.53\,\text{sec}^{-1}$, $C_0 = 1.80$, system 11.
6: rod, $G = 0.55\,\text{sec}^{-1}$, $C_0 = 1.24$, system 2.
7: rod, $G = 0.57\,\text{sec}^{-1}$, $C_0 = 0.54$, system 2.

experiments G was sufficiently low to rule out the presence of secondary flows, and sedimentation during the time of a run was negligible. Thus the drift in C' could only be due to non-*Newtonian* behaviour of the fluids.

(iv) *Rotation of discs in elasticoviscous media:* Previous work (2) with discs in elasticoviscous solutions of polyisobutylene undergoing tube flow had shown that the particles rotated according to eq. [11]. Similar results were here obtained with discs rotating in 2% aqueous polyacrylamide solutions subjected to *Couette* flow *provided* that the shear rate was below a certain critical value which, as shown in table 4 decreased with increasing particle diameter. Above this critical G the discs oriented themselves with their axis of revolution along the X_2-axis, $\varphi_1 = 0$, $\theta_1 = 90°$ and, as illustrated in fig. 5b, *ceased to rotate*

Table 4. Critical velocity gradient and torque for discs rotating in an elasticoviscous solution of 2% polyacrylamide

Diameter 2b cm	Thickness 2a cm	r_p	r_e	G[1] (crit.) sec^{-1}	η_0[2] Poise	Γ_1[3] dyne cm $\times 10^4$
0.072	0.008	0.11	0.21	6.35	11.1	1.06
0.115	0.020	0.18	0.29	3.75	13.1	4.08
0.121	0.019	0.16	0.28	1.58	16.0	2.21
0.134	0.015	0.12	0.24	0.93	17.1	1.60
0.174	0.016	0.091	0.15	0.53	17.9	2.32
0.182	0.012	0.064	0.14	0.29	18.7	1.17
0.188	0.168	0.096	0.17	0.31	18.6	1.54

[1]) Calculated assuming *Newtonian* behaviour.
[2]) Extrapolated for low G from the viscosity-rate of shear relation.
[3]) Torque calculated from eq. [18].

further. They remained aligned with the direction of the flow even when the velocity gradient was further increased. The drift in the angle θ_1 to 90° occurred even when the discs were initially in the φ_1-orientation = 0°. This is shown in fig. 8c for a disc having $r_e = 0.15$, for which C' was 2.36 when φ_1 reached 0°, after which θ_1 continuously increased to 90° with φ_1 constant.

The alignment of discs is most likely due to the elastic properties of the polyacrylamide solutions which increase with increasing polymer concentration and which, during shear give rise to a restoring torque opposing that due to viscous deformation of the fluid. When the particles cease to rotate, the two torques balance each other. Table 4 lists values of the hydrodynamic torque Γ_1 at the critical G calculated from *Jeffery's* theory (5) for a spheroid in a *Newtonian* liquid in the orbit $C = \infty$ (no spin), using the relation (21):

$$\Gamma_1 = \frac{8\pi\,\eta_0 G}{3\,\alpha_2}. \qquad [18]$$

Here α_2 is an integral, whose value for a cylinder has been shown to be:

$$\alpha_2 = \frac{A}{a\,b^2}, \qquad [19]$$

where

$$A = \frac{r_e \cos^{-1} r_e}{(1 - r_e^2)^{3/2}} - \frac{r_e^2}{1 - r_e^2}. \qquad [20]$$

As G is further increased, the particle remains at a constant orientation indicating that the elastic torque is increasing faster than the hydrodynamic torque.

A similar alignment of rods in the direction of flow was not observed as here the particles oriented themselves with the axis of re-

volution (and major axis) parallel to the vorticity or X_1-axis and were observed to spin about their axes.

c) Deformation and break-up of liquid drops

As previously found in *Newton*ian (22) and elasticoviscous fluids (2), spherical drops in all the systems listed in table 2 were deformed into ellipsoids in shear flow, and the deformation increased with increasing velocity gradient. At high G, the drops were observed to break-up and, as indicated in table 2 and described later, could be grouped into various classes according to their mode of break-up (22).

The motion of a neutrally buoyant fluid drop of radius b and viscosity η_1, suspended in a *Newton*ian liquid of viscosity η_0, subjected to *Couette* flow, was first treated by *Taylor* (23). He showed that the drop behaviour depends only on the two dimensionless parameters $\lambda = \eta_1/\eta_0$ and $\varkappa = \gamma/Gb\eta_0$, γ being the interfacial tension. To achieve a balance between the interfacial tension and the normal components of the viscous stress acting across the interface the drop undergoes a change of curvature, becoming an ellipsoid having major and minor axes L and B respectively, as shown in fig. 10a.

Two cases were considered

(i) The interfacial tension effects are dominant over the viscous effects: $\lambda = 0(1)$, $\varkappa \gg 1$, with the result that the geometrical deformation $D = L - B/L + B$ is given by:

$$D = E = \frac{f(\lambda)}{\varkappa} = \frac{Gb\eta_0}{\gamma} \cdot f(\lambda), \qquad [21]$$

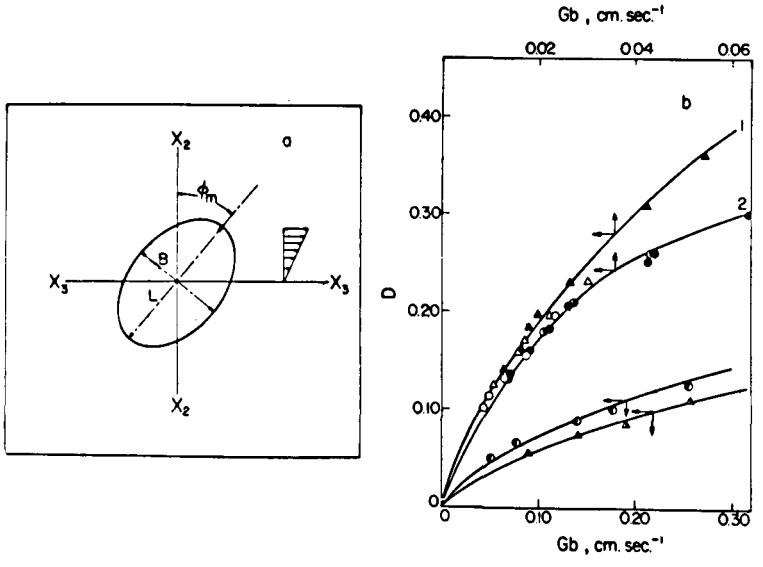

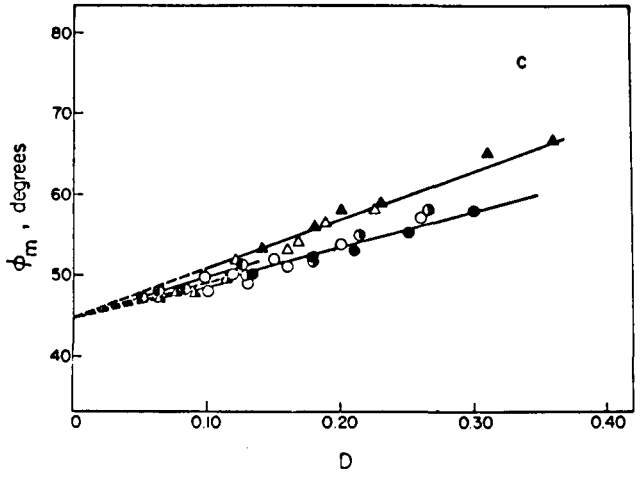

Fig. 10. (a) Coordinate system for the deformation of a drop situated at the origin of a field of *Couette* flow, $U_3 = GX_2$. – (b) Deformation of *Newton*ian drops in a pseudoplastic liquid as a function of Gb. System 13, line 2: open circles, $b = 0.050$ cm; closed circles, $b = 0.064$ cm; half open circles, $b = 0.074$ cm. System 14, line 1: open triangles, $b = 0.058$ cm; closed triangles, $b = 0.069$ cm. System 15: half open circles, $b = 0.080$ cm. System 16: half open triangles, $b = 0.065$ cm. The curves are the best fit through the experimental points. – (c) Variation of the angle of deformation for the same systems as in (b). The lines are also the best fit through the experimental points

where E is the ratio of surface tension to viscous forces, and

$$f(\lambda) = \frac{19\lambda + 16}{16\lambda + 16}. \qquad [22]$$

The drop major axis is oriented at an angle $\varphi_1 = \varphi_m = \pi/4$ (fig. 10a).

(ii) The interfacial tension effects are negligible compared to the viscous effects: $\lambda \gg 1$, $\varkappa = 0(1)$, in which case

$$D = \frac{5}{4\lambda}, \qquad [23]$$

and the drop aligns itself with the flow, $\varphi_m = \pi/2$. Eqs. [21] to [23] are valid for very small deformations only, although experiments in *Newtonian* systems (22) have sometimes given good agreement with the theory at values of $D > 0.2$. *Chaffey* and *Brenner* (24), taking into account second order terms in the deformation have treated case (i) and found that φ_m increases with D according to the relation

$$\varphi_m = \frac{\pi}{4} + \left(\frac{3}{5} + \frac{2\lambda}{5}\right) D. \qquad [24]$$

Cox (25) has recently given a more general treatment of the theory applicable to intermediate values of λ and $\varkappa$ for which φ_m, at equilibrium, lies between $\pi/4$ and $\pi/2$. The relations for D and φ_m were found to be

$$D = \frac{5(19\lambda + 16)}{4(\lambda + 1)\sqrt{(20\varkappa)^2 + (19\lambda)^2}}, \qquad [25]$$

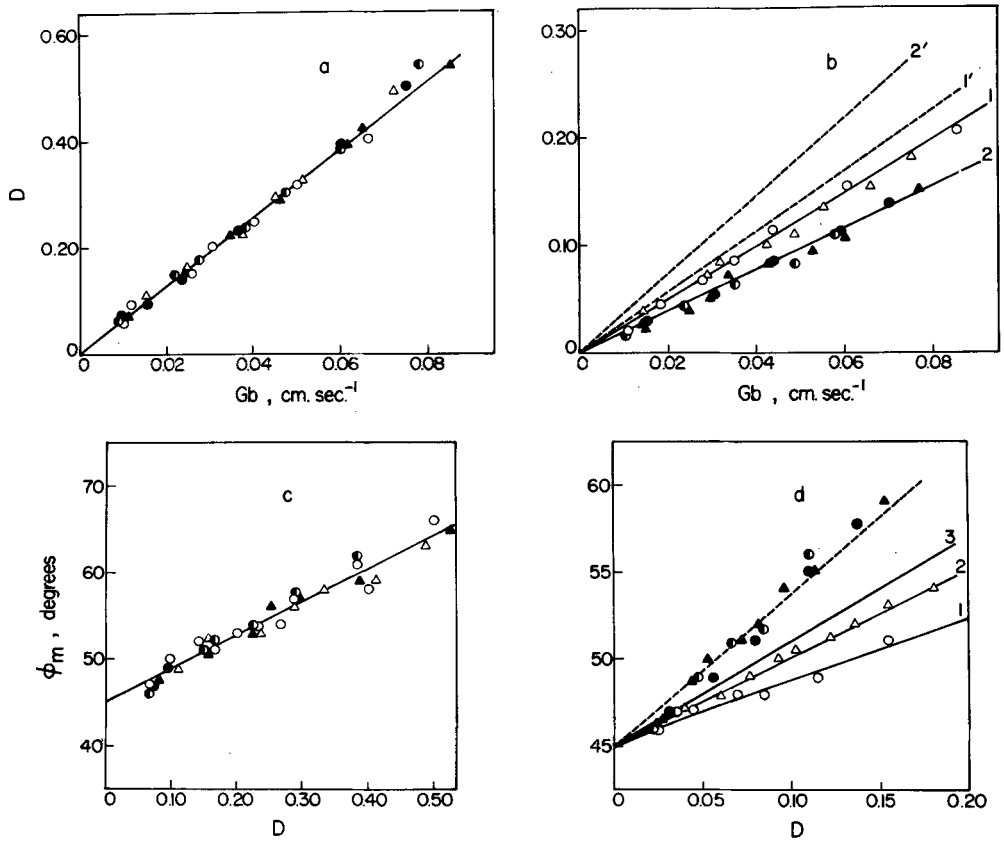

Fig. 11. Upper part: (a) Deformation of pseudoplastic drops in a *Newtonian* liquid. *Newtonian* drops, system 19: open circles, $b = 0.063$ cm. System 20: closed circles, $b = 0.069$ cm; half open circles, $b = 0.080$ cm. System 21: open triangles, $b = 0.092$ cm. System 22: closed triangles, $b = 0.088$ cm. The line was calculated for system 19 using eq. [21]. (b) Deformation of elasticoviscous drops in a *Newtonian* liquid. *Newtonian* drops, system 23: open circles, $b = 0.081$ cm. The remaining points are: system 24: open triangles, $b = 0.074$ cm, system 25: half open circles, $b = 0.055$ cm; closed circles, $b = 0.067$ cm; closed triangles, $b = 0.088$ cm. The lines 1, 1′, 2′ were calculated using eq. [21] for systems 23, 24, 25. Line 2 is the best fit through the experimental results for system 25. – Lower part: (c) Variation of φ_m with D for the same systems as in (a). The line is calculated from eq. [24] for system 19. (d) Variation of φ_m with D for the same systems as in (b). Lines 1 and 2, are calculated from eq. [24] for systems 23 and 24 respectively and line 3 is calculated from eq. [26] for system 25. The dashed line is the best fit through the experimental results for system 25

$$\varphi_m = \frac{\pi}{4} + \frac{1}{2}\tan^{-1}\left(\frac{19\lambda}{20\varkappa}\right). \qquad [26]$$

For the special cases given above, eq. [25] reduces to eq. [21] and [23] respectively, and φ_m in eqs. [26] assumes the limiting values $\pi/4$ and $\pi/2$.

(i) *Newtonian drops:* The results for *Newtonian* drops in a pseudoplastic liquid, systems 13 to 16, are shown in fig. 10 where the deformation D has been plotted against Gb. Although the points obtained at different drop diameters in each system fitted on a single curve (e.g., curves 1 and 2) as predicted by theory, a linear relation between D and Gb was not found, presumably because η_0 decreased with increasing G leading to an increased λ and hence E in eq. [21].

The variation of the angle φ_m with D for drops in the same system is shown plotted in fig. 10c. The lines, which are the best fit through the experimental points, have an intercept at $\varphi_m = \pi/4$ for $D = 0$ as predicted by eqs. [24] and [26], and found in *Newtonian* systems (22). This contrasts with the behaviour of drops in elasticoviscous liquids (2) where for $D = 0$, the intercept of φ_m on the D-axis was 61° showing an increased alignment of the major axis of the ellipsoid with the direction of flow.

(ii) *Non-Newtonian drops:* The results for the deformation of pseudoplastic and elasticoviscous drops in *Newtonian* liquids are shown in fig. 11a and 11b. In these systems the values of λ and $\varkappa$ were such that eq. [21] is a good approximation of eq. [25]. The line in fig. 11a was calculated from eq. [21] for the *Newtonian* system of pure propylene glycol drops in silicone oil, and the points are experimental. It is evident that, except at high Gb, the data obtained with pseudoplastic drops also lay on this line, a result which is in accord with eq. [21] since the respective calculated slopes $= (\eta_0/\gamma)f(\lambda)$, in systems 20, 21, and 22 are only 5%, 3% and 0.5% different from that in system 19. Similarly, the angles of orientation φ_m plotted in fig. 11c fitted, within experimental error, around the line calculated from eq. [24].

In contrast to pseudoplastic drops, the measured deformation of elasticoviscous drops of aqueous polyacrylamide in *Newtonian* liquids, while still a function of Gb, was less than predicted by *Cox*s theory. This is illustrated in fig. 11b where the points for the *Newtonian* system of water in silicone oil lie on line 1, calculated from eq. [25]. But so do the experimental points in system 24 for which the calculated slope should be 10% higher as shown by the dashed line 1′. In 4% aqueous polyacrylamide, system 25, the points at different drop diameters lie on a single line [2] actually having a lower slope than line 1 although the initial theoretical slope is 40% higher, as indicated by the calculated dashed curve 2′. This behaviour may be due to the existence of normal stresses and/or elastic recovery of the liquid inside the drops which act to decrease the deformation. The φ_m-orientations of elasticoviscous drops are shown in fig. 11d. Again, the points obtained in the *Newtonian* system 23 give a good fit of eq. [24] (line 1), and unlike the deformation, the measured φ_m of elasticoviscous drops in system 24 having a low λ agree quite well with theory as is illustrated by line 2 which was calculated from eq. [24] assuming a constant λ in the range of G used (0–2 sec^{-1}), but actually measured at $G = 3.11\ \text{sec}^{-1}$. In system 25, λ is too great to permit comparison with the second order theory of *Chaffey* and *Brenner*, and the results are seen to lie on a line having an appreciably greater slope than that calculated from eq. [26].

Nevertheless, the experimental results show that, as predicted by the theory (24, 25), at a given deformation, the alignment of the deformed drop with the flow is greater at higher λ.

(iii) *Break-up of drops:* Table 2 shows that the values of λ in the suspensions of liquid drops varied from 2×10^{-4} to 2.8 and, as in *Newtonian* liquids in this range of λ (22), drop break-up in Classes A, B-1 and B-2 was observed[4]). When $\lambda < 10^{-2}$ break-up occurred in Class A with the drops developing pointed ends and the liquid being ejected at the two extremities. System 25, in which $\lambda = 2.8$, showed Class B-2 break-up in which the elasticoviscous drops extended into long threads which only broke up into small droplets when the apparatus was stopped. The remaining systems all having $\lambda < 1$, belonged to Class B-1 in which the drops were pulled out until a neck was formed between their rounded ends, which then separated to form two parent drops with three satellite droplets between them. This behaviour paralleled that previously found in

[4]) Recent work by *Torza* et al. (26) has shown that drops exhibiting Class A break-up are in unstable equilibrium, as a result of too rapid an increase in the velocity gradient. When G is increased very slowly and the drops are always in true equilibrium, Class B-1 break-up is observed in these systems.

*Newton*ian systems and with *Newton*ian drops in polyacrylamide solution (2).

Measurements of the velocity gradient at break-up, G_B, were made and are listed in table 5 together with the deformation at burst, E_B, calculated from eq. [21] using the measured apparent viscosities of the drop fluid at G_B. It may be seen that in a given system the values of $G_B b$ were independent of b. The mean values of E_B for pseudoplastic drops lay at the top of the range previously found for *Newton*ian systems ($\bar{E}_B = 0.52 \pm 0.10$). In the case of the elasticoviscous drops of system 24, $\bar{E}_B$ was considerably higher, and this, as the abnormally low deformability reported above, was probably due to the effects of normal stresses in the polyacrylamine solution.

d) Migration of rigid and deformable particles

(i) *Rigid spheres:* Previous experiments (2) had shown that rigid spheres suspended in an elasticoviscous fluid subjected to *Couette* flow migrated towards the outer cylinder. It was suggested that since the velocity gradient was greater at the inner cylinder than at the outer, a pressure difference due to the normal stresses would result in a force pushing the spheres towards the outer cylinder. In the present experiments with pseudoplastic liquids, the opposite behaviour was found: the particles migrated towards the inner cylinder, i.e. towards the region of greater velocity gradient. As described elsewhere (4), a similar result was obtained in tube flow where rigid particles migrated towards the tube wall, whereas in elasticoviscous liquids they had been found to migrate towards the tube axis (2). The results in *Couette* flow are illustrated in fig. 12 and it is evident that the direction of migration was independent of which cylinder was stationary (curves 1 and 3) and of the direction of rotation (curves 1 and 2). The rates of migration increased with the sphere diameter (curves 1 and 5) and also with the velocity gradient (curves 1 and 2). Surprisingly, however, when the particles were close to the outer cylinder

$$[(R - R_I)/(R_{II} - R_I) > 0.75],$$

they migrated towards it (curve 4). In all experiments G was less than 8 sec^{-1}, and as shown in fig. 2, there are no measurable normal stresses at this value of the shear rate. In addition, great care was taken to avoid secondary flows in the annulus of the *Couette* apparatus which might have accounted for radial migration. A low viscosity (0.01 Poise) mixture of silicone oil and carbon tetrachloride was used as bottom layer, on which the propylene glycol solution (η_0 = 6.9 Poise) was floated. In all cases, the sedimentation rates were less than 0.1 cm/h

Table 5. Velocity gradient at burst of non-*Newton*ian drops suspended in a *Newton*ian liquid

System 19			System 20			System 21		
b cm	G_B [1] sec^{-1}	$G_B b$ cm sec^{-1}	b cm	G_B [1] sec^{-1}	$G_B b$ cm sec^{-1}	b cm	G_B [1] sec^{-1}	$G_B b$ cm sec^{-1}
0.028	4.11	0.11	0.042	2.48	0.12	0.031	2.81	0.09
0.040	1.91	0.08	0.053	1.84	0.10	0.040	2.60	0.10
0.051	1.84	0.09	0.073	1.44	0.11	0.050	1.95	0.10
0.063	1.68	0.11	0.092	1.11	0.10	0.064	1.33	0.09
0.106	0.96	0.10	0.156	0.87	0.10	0.080	1.02	0.08
Average: $\overline{G_B b} = 0.10$				$\overline{G_B b} = 0.10$			$\overline{G_B b} = 0.91$	
$\bar{E}_B$ [2] $= 0.61$				$\bar{E}_B$ [2] $= 0.65$			$\bar{E}_B$ [2] $= 0.59$	

System 23			System 24		
0.043	5.18	0.20	0.033	8.20	0.27
0.055	3.57	0.21	0.041	6.10	0.26
0.073	3.19	0.23	0.052	4.79	0.25
0.087	2.61	0.19	0.066	4.02	0.26
0.114	1.79	0.22	0.083	3.04	0.26
Average: $\overline{G_B b} = 0.22$				$\overline{G_B b} = 0.26$	
$\bar{E}_B$ [2] $= 0.54$				$\bar{E}_B$ [2] $= 0.73$	

[1]) G_B velocity gradient at burst.
[2]) $\bar{E}_B$ calculated deformation at burst from $\overline{G_B b}$ using the measured drop apparent viscosity, and eq. [21].

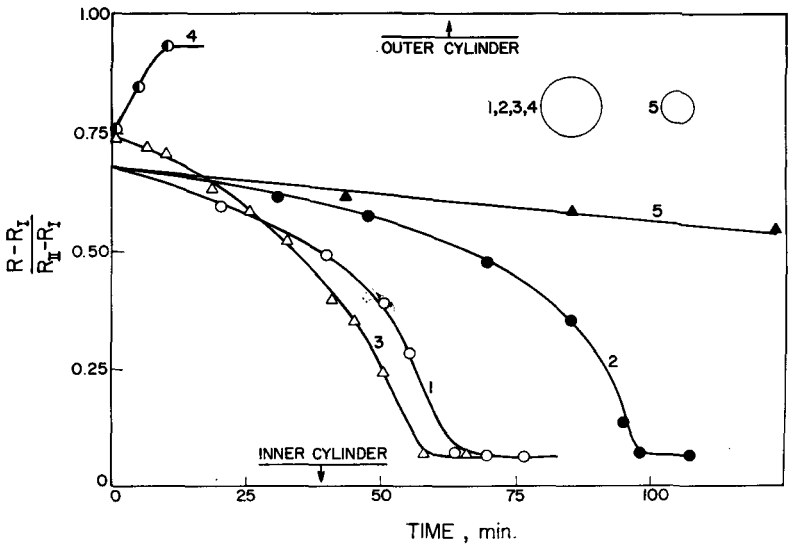

Fig. 12. Migration of rigid particles in a pseudoplastic liquid in *Couette* flow, system 4, $R_I = 4.756$ cm, $R_{II} = 5.652$ cm. Curves 1 to 4: $b = 0.056$ cm; curve 1: $\Omega_I = 0$, $\Omega_{II} = -1.07$ rad. sec^{-1}, $G = 7.32$ sec^{-1}; curve 2: $\Omega_I = 0$, $\Omega_{II} = -0.748$ rad. sec^{-1}, $G = 5.13$ sec^{-1}; curves 3 and 4: $\Omega_I = 1.07$ rad. sec^{-1}, $\Omega_{II} = 0$, $G = 5.20$ sec^{-1}; curve 5: $b = 0.032$ cm, $\Omega_I = 0$, $\Omega_{II} = 1.07$ rad. sec^{-1}, $G = 7.32$ sec^{-1}. The size of the spheres relative to the gap width is also shown; positive and negative signs of Ω indicate counter-clockwise and clockwise rotation of the cylinders respectively. The values of G are those calculated at the stationary layer or at the resting inner cylinder

for a sphere ($b = 0.02$ cm) located in the middle of the annulus. Moreover, during the experiments, the spheres did not sink or rise at a rate greater than the one observed without shear. *Taylor* (27) in a study of the secondary flows between two cylinders rotating in the same direction found that they were a succession of alternate vortices of opposite direction extending from one cylinder to the other. When the cylinders counter-rotated, the vortices developed in two regions of the annulus, one close to the inner cylinder and the other close to the outer with the circulation still changing direction from one vortex to the other as if they were geared together. Consequently, in the presence of secondary flows, the particles would be expected to migrate towards the inner or outer cylinders and also upwards and downwards depending on their initial position of release in the annulus. This behaviour was not observed during the course of the above experiments where, at a given G, the direction and rate of migration were the same when a sphere was located at different heights but at the same radial distance R in the annulus.

(ii) *Deformable drops:* In both elasticoviscous and pseudoplastic liquids as shown in fig. 13a and 13b respectively, fluid drops migrated away from the cylinder walls towards an equilibrium position. The rates of migration increased with increasing velocity gradient and the ratio $b/(R_{II}-R_I)$ and decreased with decreasing radial distance from the equilibrium position. The position of equilibrium was itself dependent on G and $b/(R_{II}-R_I)$, being closer to the inner cylinder for drops suspended in a pseudoplastic liquid and closer to the outer cylinder for drops in an elasticoviscous medium.

Two-way migration of deformable drops in *Couette* flow had previously been observed in *Newton*ian systems (28), but there the equilibrium position was about half-way between the cylinders and the phenomenon was explained as resulting from a combination of the particle deformation and its interaction with the wall (29, 30). In non-*Newton*ian media, presumably, there is superimposed on the wall migration, the migration observed with rigid spheres, and this results in a displacement of the equilibrium position towards one or other of the cylinders.

e) Collision of spheres

In *Newton*ian liquids at low *Reynolds* numbers, two-body collisions between rigid spheres are found to be symmetrical and reversible (31, 32). The particles approach along curvilinear paths and, after coming into apparent contact with each other, rotate as a rigid dumbbell, until they separate at an orientation φ_1 of the axis joining their centers, which is the reflection of the angle of contact. The spheres then recede along curvilinear paths which are the mirror image of the paths of approach. If the flow is now reversed, the spheres recollide along paths which are the exact reverse in time and space of those followed in the forward collision.

In elasticoviscous liquids, however, two-body collisions, between rigid spheres are

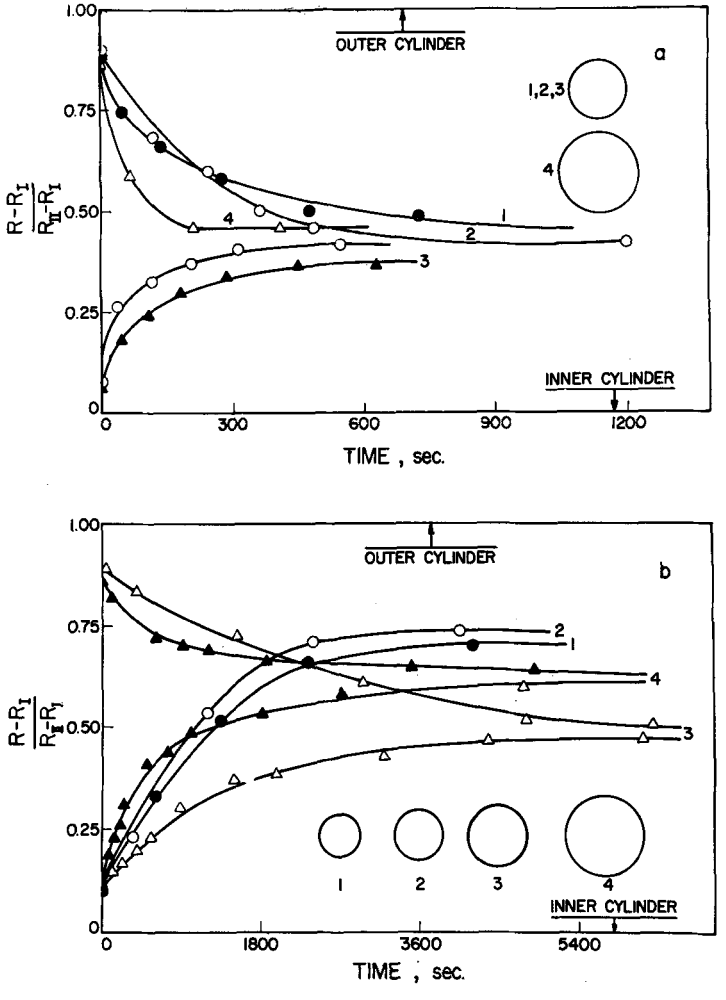

Fig. 13. Migration of liquid drops in *Couette* flow. $R_I = 4.756$ cm, $R_{II} = 5.652$ cm. (a) Suspending phase: Pseudoplastic liquid, system 17. Curves 1–3:
$b = 0.066$ cm, open circles:
$\Omega_I = 0.495$ rad. sec^{-1}, $\Omega_{II} = 0$,
$G = 2.40$ sec^{-1}; closed circles:
$\Omega_I = 0$, $\Omega_{II} = -0.293$ rad. sec^{-1},
$G = 2.01$ sec^{-1}; closed triangles:
$\Omega_I = 0.281$ rad. sec^{-1},
$\Omega_{II} = 0$, $G = 1.36$ sec^{-1}.
Curve 4, open triangles:
$b = 0.091$ cm, $\Omega_I = 0.495$ rad. sec^{-1}, $\Omega_{II} = 0$, $G = 2.40$ sec^{-1} (b) Suspending phase: Elasticoviscous liquid, system 18. Open circles b: = 0.043 cm, $\Omega_I = 0.144$ rad. sec^{-1}, $\Omega_{II} = -0.143$ rad. sec^{-1}, $G = 1.68$ sec^{-1}; closed circles: $b = 0.054$ cm, $\Omega_I = 0.144$ rad. sec^{-1}, $\Omega_{II} = -0.143$ rad. sec^{-1}, $G = 1.68$ sec^{-1}; open triangles: $b = 0.064$ cm, $\Omega_I = 0.061$ rad. sec^{-1}, $\Omega_{II} = -0.062$ rad. sec^{-1}, $G = 0.72$ sec^{-1}; closed triangles: $b = 0.083$ cm, $\Omega_I = 0.151$ rad. sec^{-1}, $\Omega_{II} = -0.102$ rad. sec^{-1}, $G = 1.43$ sec^{-1}. – The size of the drops relative to the gap is also shown: positive and negative signs of Ω refer to counter-clockwise and clockwise rotation of the cylinders respectively, and the values of G were calculated at the stationary layer or at the stationary cylinder

found to be unsymmetrical and irreversible (2). The same behaviour was here observed in pseudoplastic media and is shown in fig. 14a in a dimensionless plot of the paths of the centers of two polystyrene spheres of equal diameter colliding in the equatorial plane, i.e. $\theta_1 = \pi/2$. It is convenient to describe the collision in terms of the rectilinear collision angles of approach, φ_a, and recession, φ_r,

$$|\varphi_a| = \cos^{-1}\left(\frac{\Delta X_2}{2b}\right), \qquad [27]$$

and similarly for φ_r. ΔX_2 is the separation of particle centres along the X_2-axis when the axial separation of centers $\Delta X_3 > 4b$. The figure shows that the paths of approach and recession were curvilinear and in the first collision $|\varphi_a|$ was greater than $|\varphi_r|$ resulting in an increased separation of their centers along the X_2-axis. Upon reversal of the flow, the spheres recollided at an angle $|\varphi_a'| = |\varphi_r|$ and separated at $|\varphi_r'| < |\varphi_a'|$ again increasing their separation. After three such collisions, the particles no longer made apparent contact. Three body collisions were also observed; as expected these were also unsymmetrical and irreversible and, as shown in fig. 14b, the values of ΔX_2 for all three spheres increased after each collision. The cause of this irreversibility, as in elasticoviscous suspending media, is probably due to the asymmetry of the forces generated by the fluid acting along the doublet axis, compressive in the quadrant of approach, and tensile in that of recession. In *Newtonian* liquids, these forces are symmetric around the X_2-axis, $\varphi_1 = 0$ (31), whereas in both elasticoviscous and pseudoplastic media this does not appear to be the case. Furthermore it appears that on reversing the rotation of the field, the magnitude as well as the sign of the force is changed.

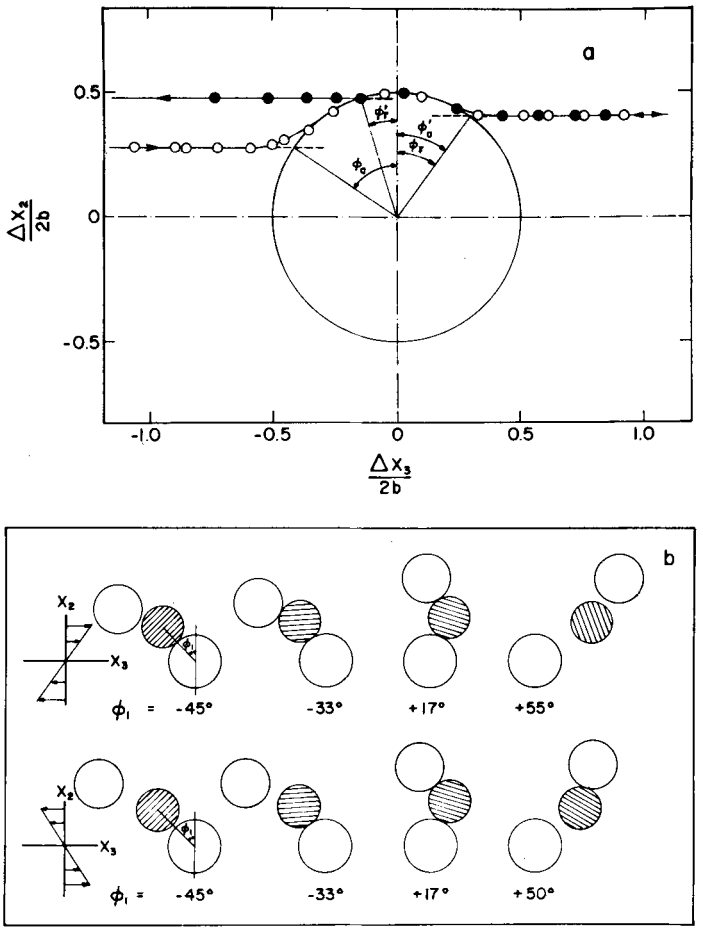

Fig. 14. Collisions of rigid spheres in *Couette* flow. (a) Dimensionless plot of the paths of particle centers about the midpoint of the doublets for an equatorial collision ($\theta_1 = \pi/2$) in a pseudoplastic liquid, system 6. The open circles are the experimental points obtained during the first collision and the closed circles those during the second collision by reversing the flow. $b = 0.058$ cm, $\Omega_I = 0.013$ rad. sec^{-1}, $\Omega_{II} = -0.007$ rad. sec^{-1}; $|\varphi_a| = 56°$, $|\varphi_r| = |\varphi_a'| = 33°$, $|\varphi_r| = 17°$. (b) Tracings from cine films illustrating the nonreversibility of a three body collision in system 8. The angles φ_1 made by the line joining the centers of the lower two spheres are the same in the corresponding sequences of the forward (upper part) and reverse collision (lower part) but the spheres separated from each other

Concluding remarks

The present Part completes a study of single particle behaviour in non-*Newtonian* fluids and it is of interest to compare the results previously obtained in *Newtonian* fluids (1) with those in elasticoviscous and pseudoplastic liquids. This information has been summarized in table 6.

Certain results are identical in all three types of fluid e.g. the measured angular velocities of spheres are found to be equal to half the velocity gradient and this, as shown in the second Part (4), is also true in *Poiseuille* flow. The modes of deformation and burst of fluid drops are also similar in the three fluids, although in an elasticoviscous suspending phase, the drop is more aligned with the direction of the flow than theory predicts.

Some of the phenomena reported with particles in elasticoviscous media (2) which differ from those in *Newtonian* fluids are also observed in pseudoplastic liquids. Thus, collisions between rigid spheres are unsymmetrical and irreversible, and the rotation of rigid rods and discs results in their adopting preferred limiting rotational orbits which, for *Newtonian* liquids, corresponds to minimum energy dissipation in *Couette* flow. It should be noted that since it was shown that the pseudoplastic fluids here used have no measurable elastic properties, and since there are no measurable normal stresses present at low experimental velocity gradients, these results must be explained in terms of other rheological properties of the fluid.

The observed adoption of limiting rotational orbits by cylinders raises the question whether it is possible to flow a suspension of rods until all particles are oriented with their major axis parallel to the fluid vorticity axis. In this case the suspension should be free flowing even at very high concentrations close to the packing volume fraction for cylinders which is between 0.78 and 0.91. However, the results of the experiments in

Table 6. Summary of particle behaviour in *Couette* flow of *Newtonian* and non-*Newtonian* liquids at low *Reynolds* numbers

	Newtonian liquids	Elasticoviscous liquids	Pseudoplastic liquids
Rotation of a rigid sphere	$2\,\omega_1/G = 1$	$2\,\omega_1/G = 1$	$2\,\omega_1/G = 1$
Angular velocity of a rigid rod	follows eq. [11]	follows eq. [11]	follows eq. [11]
Angular velocity of a rigid disc	follows eq. [11]	follows eq. [11] at low G in polyacrylamide solutions; rotation ceases at higher G depending on polymer conc. and disc size	follows eq. [11]
Drift in the orbit constant of a rod	C = constant	$C' \to 0$	$C' \to 0$
Drift in the orbit constant of a disc	C = constant	$C' \to \infty$	$C' \to \infty$
Deformation and burst of liquid drops			
Newtonian drop	follows equation [26]; classes A, B, C burst	theory not obeyed; classes A, B and C burst	theory not obeyed; classes A and B burst
Elasticoviscous drop	D less than given by eq. [26]; only class B burst observed		
Pseudoplastic drop	follows eq. [26]; only class B burst observed		
Orientation of liquid drops			
Newtonian drop	at low λ, follows eq. [24]; at high λ, follows equation [26]	at $D = 0$, $\varphi_m = \pi/4$; at higher D, theory not obeyed	at low λ, follows eq. [24]
Elasticoviscous and pseudoplastic drops	at low λ, follows eq. [24]		
Lateral migration of rigid spheres	none	towards lower G, i.e. to the outer cylinder	towards lower G (inner cylinder) except for $\frac{R - R_I}{R_{II} - R_I} < 0.75$ when migration is to outer cylinder
Lateral migration of liquid drops	away from the cylinder walls to the center of the annulus	away from the walls, equilibrium closer to the outer cylinder	away from the walls, equilibrium closer to inner cylinder
Collision of rigid spheres	symmetrical and reversible	unsymmetrical and irreversible	unsymmetrical and irreversible

which the distribution of orientations of rods were studied in suspensions from 0.03 to 20% volume concentration, and which are described in another paper (33), have shown that such a situation is not realized in practice. Thus, the mean values of the projection $r_{23} = \sin\theta_1$ of unit length of the rods in the X_2X_3-plane show that $\bar{r}_{23}$ is never very close to 0, corresponding to perfect alignment with the X_1-axis, increasing from 0.326 at $c = 1.5\%$ to 0.686 at $c = 20\%$, a value approaching that, 0.785, calculated for a random distribution (34). These results indicate that interactions between the rods play a very important role in determining their equilibrium orientations.

The most striking difference in particle behaviour between the two non-*Newtonian* media is in the migration of rigid and deformable spheres. The astonishing reversal of the direction of lateral motion in going from elasticoviscous to pseudoplastic liquids, even more strikingly revealed in the non-uniform velocity gradient existing in *Poiseuille* flow (4), cannot be explained at present. The suggestion that the combined action of the velocity gradient and normal stresses can account for particle migration (8) appears now to be oversimplified.

Also of great interest is the observed alignment with the direction of the flow of discs in elasticoviscous solutions at sufficiently high shear rates and polymer concentrations. It appears that this can be explained by postulating a balance between the torque due to elastic deformation of the

fluid, and that due to viscous deformation. The result is similar to that observed in the rotation of cylinders under the combined action of a shear and electric field (35), except that there, a series of steady state values of φ_1 are possible depending on the ratio of electrical field strength to velocity gradient as well as on r_e. The existence of an elastic restoring stress may also account for the observed lower deformability of elasticoviscous drops in *Newtonian* suspending fluids.

Summary

An experimental study of the behaviour of rigid and deformable particles suspended in pseudoplastic and elasticoviscous liquids undergoing slow *Couette* flow was undertaken. The velocity profiles deviated slightly from those obtained for *Newtonian* fluids, but the measured angular velocities of rigid spheres showed that the rotation of the field was equal to half the velocity gradient. While the measured angular velocities of rods and discs were in accord with theory applicable to *Newtonian* liquids, in both non-*Newtonian* media there was a steady drift in the orbit towards an asymptotic value corresponding to minimum energy dissipation in the flow. Furthermore, discs in elasticoviscous solutions of polyacrylamide at higher shear stresses aligned themselves in the direction of the flow and ceased to rotate.

Migration of rigid particles across the planes of shear in the annulus of the *Couette* was also observed. In pseudoplastic liquids, the migration was towards the region of higher shear, whereas the opposite was true in elasticoviscous liquids.

The deformation, orientation and burst of pseudoplastic drops in *Newtonian* liquids and that of *Newtonian* drops in pseudoplastic fluids were similar to those previously in completely *Newtonian* systems. With elasticoviscous drops, however, the deformation was smaller than given by theory.

As in elasticoviscous fluids, two-body collisions of rigid uniform spheres in the pseudoplastic liquids were unsymmetrical and irreversible, thus differing from collisions in *Newtonian* systems where complete reversibility is observed.

While some of the observed phenomena in elasticoviscous suspensions could be qualitatively interpreted, particle behaviour in the pseudoplastic liquids could not be explained in terms of the known rheological properties of the fluids.

Zusammenfassung

Es wurde experimentell das Verhalten von festen und deformierbaren Teilchen untersucht, die bei der Suspension in strukturviskosen und viskoelastischen Flüssigkeiten einer langsamen *Couette*-Strömung ausgesetzt sind. Die Geschwindigkeitsprofile zeigten gewisse Abweichungen von denen *Newton*scher Flüssigkeiten, aber die gemessenen Winkelgeschwindigkeiten der festen Kügelchen ergaben, daß die Drehung des Feldes gleich dem halben Geschwindigkeitsgradienten war. Die gemessenen Winkelgeschwindigkeiten der Stäbchen und Scheiben stimmten mit der Theorie, die auf *Newton*sche Flüssigkeiten zutrifft, überein. In beiden nicht-*Newton*schen Flüssigkeiten verschob sich jedoch die Kreisbahn stetig zu einem asymptotischen Wert, der einem Minimum der Dissipationsenergie der Strömung entsprach. Scheibchen in viskoelastischen Lösungen von Polyacrylamid richteten sich bei höherer Scherspannung in Strömungsrichtung aus und zeigten keine Drehung mehr.

Es wurden auch Wanderungen von festen Teilchen über die Scherebene im Spalt der *Couette*-Anordnung beobachtet. In strukturviskosen Flüssigkeiten erfolgte die Wanderung in Richtung der höheren Scherung, während auf elastische Flüssigkeiten das Gegenteil zutraf.

Die Deformation, Orientierung und das Aufbrechen strukturviskoser Tröpfchen in *Newton*schen Flüssigkeiten und das Verhalten von *Newton*schen Tröpfchen in strukturviskosen Flüssigkeiten waren den früher in rein-*Newton*schen Systemen beobachteten Phänomenen ähnlich. Die Deformation der viskoelastischen Tröpfchen war jedoch kleiner als die von der Theorie vorhergesagt worden war.

Zweikörper-Zusammenstöße zwischen festen gleichförmigen Kügelchen in strukturviskosen Flüssigkeiten waren unsymmetritch und irreversibel. Darin unterschieden sie sich von Zusammenstößen in *Newton*schen Flüssigkeiten, in denen völlige Umkehrbarkeit beobachtet worden war.

Während einige der beobachteten Phänomene in viskoelastischen Suspensionen qualitativ gedeutet werden konnten, ließ sich das Teilchenverhalten in strukturviskosen Flüssigkeiten nicht anhand der bekannten rheologischen Eigenschaften der Flüssigkeiten erklären.

References

1) *Goldsmith, H. L.* and *S. G. Mason*, in: *F. R. Eirich*, ed., Vol. 4, Chapter 2, 85–250, Rheology: Theory and Applications (New York 1967).

2) *Karnis, A.* and *S. G. Mason*, Trans. Soc. Rheol. **10**, 571 (1967).

3) *Reiner, M.* and *Scott, Blair, G. W.*, in: *F. R. Eirich*, ed., Vol. 4, Chapter 9, 461–488, Rheology: Theory and Applications (New York 1967).

4) *Gauthier, F. J., H. L. Goldsmith*, and *S. G. Mason*, Trans. Soc. Rheol. **15**, 297 (1971).

5) *Jeffery, G. B.*, Proc. Roy. Soc. (London) **A102**, 161 (1922).

6) *Brenner, H.*, Adv. Chem. Eng. **6**, 287 (1965).

7) *Taylor, G. L.*, Proc. Roy. Soc. (London) **A 138**, 41 (1932).

8) *Eringen, C. A.*, Nonlinear Theory of Continuous Media, p. 221–249 (New York 1962).

9) *Bird, R. B., W. E. Stewart*, and *E. W. Lightfoot*, in: Transport Phenomena, Chapter I, 11 (New York 1966).

10) *Darabaner, C. L., J. K. Raasch*, and *S. G. Mason*, Can. J. Chem. Eng. **45**, 3 (1967).

11) *Weissenberg, K.*, Nature **159**, 310 (1947).

12) *Dodge, D. W.* and *A. B. Metzner*, Amer. Ind. Chem. Eng. J. **5**, 189 (1959).

13) *Fisher, W. H., W. H. Bauer*, and *S. E. Wisberley*, Trans. Soc. Rheol. **5**, 221 (1961).

14) *Princen, H. M., I. Y. Z. Zia*, and *S. G. Mason*, J. Colloid Interface Sci. **23**, 99 (1966).

15) *Trevelyan, B. J.* and *S. G. Mason*, J. Colloid Sci. **6**, 354 (1951).

16) *Goldsmith, H. L.* and *S. G. Mason*, J. Fluid Mech. **12**, 88 (1962).

17) *Anczurowski, E.* and *S. G. Mason*, Trans. Soc. Rheol. **12**, 204 (1968).

18) *Anczurowski, E.* and *S. G. Mason*, J. Colloid Interface Sci. **23**, 533 (1967).

19) *Anczurowski, E.* and *S. G. Mason*, J. Colloid Interface Sci. **23**, 522 (1967).

20) *Saffman, P. G.*, J. Fluid Mech. **1**, 540 (1956).
21) *Chaffey, C. E.* and *S. G. Mason*, J. Colloid Sci. **20**, 330 (1965).
22) *Rumscheidt, F. D.* and *S. G. Mason*, J. Colloid Sci. **16**, 238 (1961).
23) *Taylor, G. I.*, Proc. Roy. Soc. (London) **A146**, 501 (1934).
24) *Chaffey, C. E.* and *H. Brenner*, J. Colloid Interface Sci. **24**, 258 (1967).
25) *Cox, R. G.*, J. Fluid Mech. **37**, 601 (1969).
26) *Torza, S., R. G. Cox*, and *S. G. Mason*, J. Colloid Interface Sci. (in press, 1972).
27) *Taylor, G. I.*, Phil. Trans. Roy. Soc. (London) **A223**, 289 (1923).
28) *Karnis, A.* and *S. G. Mason*, J. Colloid Interface Sci. **24**, 164 (1967).
29) *Chaffey, C. E., H. Brenner*, and *S. G. Mason*, Rheol. Acta **4**, 56 (1965).
30) *Chaffey, C. E., H. Brenner*, and *S. G. Mason*, Rheol. Acta **4**, 64 (1965), and correction ibid. **6**, 100 (1967).
31) *Allan, R. S.* and *S. G. Mason*, J. Colloid Sci. **17**, 383 (1962).
32) *Darabaner, C. L.* and *S. G. Mason*, Rheol. Acta **6**, 273 (1967).
33) *Gauthier, F. J., H. L. Goldsmith*, and *S. G. Mason*, Kolloid-Z. u. Z. Polymere (in press, 1971).
34) *Anczurowski, E., R. G. Cox*, and *S. G. Mason*, J. Colloid Interface Sci. **23**, 547 (1967).
35) *Chaffey, C. E.* and *S. G. Mason*, J. Colloid Sci. **19**, 525 (1964).

Authors' address:
F. Gauthier, H. L. Goldsmith, and *S. G. Mason*,
Pulp and Paper Research Institute of Canada
Dept. of Chemistry
McGill University, Montreal (Canada)